IEEE Access
Multidisciplinary | Rapid Review | Open Access Journal

IEEE RELIABILITY SOCIETY SECTION

Received 22 January 2024, accepted 16 February 2024, date of publication 21 February 2024, date of current version 1 March 2024.

Digital Object Identifier 10.1109/ACCESS.2024.3368860

RESEARCH ARTICLE

Posterior Error Energy Minimization Based Combined FxNLMS and FxLMS Algorithm for Active Noise Control

YUNHE PANG, SHIFENG OU, ZHUORAN CAI, (Member, IEEE), AND YING GAO
School of Physics and Electronic Information, Yantai University, Yantai 264005, China

Corresponding author: Ying Gao (claragaoying@126.com)

This work was supported in part by Shandong Provincial Natural Science Foundation under Grant ZR2022MF314.

ABSTRACT The filtered-x normalized least mean square (FxNLMS) algorithm is widely used in active noise control (ANC) systems. However, for cyclostationary input signals, the noise reduction performance of the FxNLMS algorithm is affected by the periodic power of cyclostationary inputs, which leads to a larger steady-state mean square deviation (MSD) than the filtered-x least mean squares (FxLMS) algorithm. In this paper, a new adaptive combination algorithm of FxNLMS and FxLMS is proposed to suppress cyclostationary input noise with fast convergence and low steady-state MSD. The mixing parameter for combining the two algorithms is obtained by minimizing the energy of the posterior error and updated using the time-average method. The mathematical analysis including the mean square convergence and computational complexity are performed. The simulation results show that the proposed combined-FxNLMS-FxLMS algorithm can efficiently combine the respective advantages of FxNLMS and FxLMS algorithms and improve the noise reduction performance of the ANC system.

INDEX TERMS Active noise control, adaptive combinations, mixing parameter, moving average.

I. INTRODUCTION

With the development of society and industry, noise pollution has attracted widespread global attention. Traditional noise control methods primarily rely on acoustic treatment, sound insulation, and the use of mufflers. These methods belong to the category of Passive Noise Control (PNC) and are typically effective against high-frequency noise. However, to address the challenge of low-frequency noise, scholars have proposed active noise control (ANC) technology [1], [2]. Currently, ANC has found widespread applications in numerous fields, including automotive engine noise control [3], aircraft cockpit noise control [4], pipe noise control [5], among others.

The adaptive filtering algorithm plays a crucial role in ANC systems. Due to its favorable performance and ease of implementation, the filtered x-normalized least mean square (FxNLMS) algorithm has been extensively adopted in various ANC systems [6]. However, it faces a limitation with its fixed step-size. This limitation makes it challenging to strike a balance between convergence speed and denoising accuracy. To resolve this limitation, several variable step-size (VSS) algorithms have been developed in recent years [7], [8], [9], [10]. Such as in [9], a variable step- size algorithm was proposed, which is based on the arctangent function. Additionally, [10] proposed the Correlation FxLMS (CFxLMS) algorithm. This algorithm utilizes the correlation function between the filtered reference signal and the error signal to regulate the updates of the step-size. In [11], the author introduced a novel error reused ANC (ErANC) system that utilizes information from past errors to compensate for the discrepancy between the main noise and the estimated output and developed a new algorithm called ErFxLMS was to enhance the noise reduction performance of the ANC system. Additionally, several filtered-x affine projection (FxAP) algorithms have been proposed to improve the convergence speed when dealing with correlated input signals. In [12], the author enhanced the algorithm performance by optimizing the regularization parameters. In [13], the author developed

The associate editor coordinating the review of this manuscript and approving it for publication was Zhaojun Steven Li.

a variable step-size strategy based on mean square error analysis and demonstrated the superiority of the algorithm through simulation experiments. Several techniques have been reported to address the challenge of impulse noise in ANC systems. The author proposed three improvement schemes in [14] to improve the performance of the filtered-x least mean absolute third (FxLMAT) algorithm. In [15], the author presented the modified filtered-x affine-projection-like MCC (MFxAPLMCC) algorithm. This algorithm is inspired by the maximum correntropy criterion (MCC) and is based on an information-theoretic learning framework and a data-reuse scheme derived from affine-projection algorithms. In [16], the Volterra filtered-x maximum correntropy criterion (VFxMCC) algorithm and Volterra filtered-x recursive maximum correntropy (VFxRMC) algorithm were employed in a non-linear active noise control system to improve the stability of the Volterra filter when dealing with impulsive noise. Lately, the convex combination scheme has gained significant attention in ANC systems. In [17], the author used sigmoid functions to formulate mixing parameters to control the proportion of the two filters and proposed the Convex Combination FxNLMS and FxLMS (CVX-FxNLMS-FxLMS) algorithm for ANC systems. In [18], a new Combined-Step-Size (CSS) algorithm was proposed using adaptive combination method, resulting in good performance while maintaining low computational complexity. However, when developing the mixing parameter, it directly utilized the variable step size factor method from [19], which lacks a theoretical basis. In [20], the author applies the general mixed-norm algorithm as the cost function to propose the filtered-x general mixed-norm (FxGMN) algorithm. To further enhance its performance, they present a convex combination of the FxGMN algorithm (C-FxGMN).

In practical applications, the input noise of ANC systems is usually mechanical vibration noise with cyclostationary characteristics such as automobile engine noise and piping noise [21], [22], [23]. For such input signals, the theoretical results have shown that the steady-state mean square deviation (MSD) of the FxNLMS algorithm is affected by the periodic input power leading to degraded noise reduction performance, while the steady-state MSD of the FxLMS algorithm is independent of the periodic input power. That is to say, FxNLMS has faster convergence but suffers from larger MSD than FxLMS for cyclostationary input noise [18], [24]. Therefore, the existing variable step-size and combined step-size schemes cannot fundamentally solve the problem of the FxNLMS algorithm suffering from large steady-state misalignment for cyclostationary input noise signals.

To fully utilize the advantages of these two algorithms in dealing with cyclostationary input noise, an adaptive algorithm combining FxNLMS and FxLMS is proposed. The algorithm combines FxNLMS and FxLMS algorithms using two different step sizes. Larger step-size in FxNLMS is used during transient periods to achieve fast convergence and good transient response, while the other smaller step- size in FxLMS is activated in steady-state for the low steady-state MSD. The mixing parameter for combining these two algorithms is obtained by minimizing the energy of the posteriori error. Besides, we use the time-average method to update the mixing parameter, which can not only ensure monotonicity but also avoid excessive fluctuation during the change of the parameter [25]. Simulation results show that the proposed algorithm can improve the performance of the ANC system, and has faster convergence speed and better noise reduction effect compared to the existing algorithms.

The structure of the remainder of this paper is as follows: Section II describes the conventional FxNLMS algorithm. Section III presents the structure and derivation process of the proposed algorithm. Section IV illustrates the mean square convergence and the computational complexity analysis. The simulation results are exhibited in the section V. Finally, section VI summarizes the conclusion.

II. THE FxNLMS ALGORITHM

The block diagram of the FxNLMS algorithm is shown in Fig. 1, where $d(n)$ is the noise signal output through the primary path to be cancelled. $P(z)$ indicates the primary path transfer function, $S(z)$ represents denotes the secondary path transfer function, and $\hat{S}(z)$ signifies the approximate estimate of $S(z)$. $W(z)$ is the ANC controller (adaptive filter). $y(n)$ is the filter output signal to activate the secondary speaker and $\mathbf{x}(n) = [x(n), x(n\text{-}1), \ldots, x(n\text{-}L+1)]^T$ is the input noise vector with the length L [26].

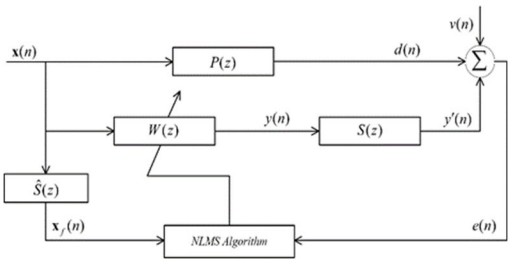

FIGURE 1. Block diagram of the FxNLMS algorithm.

The filter output signal $y(n)$ is given by

$$y(n) = \mathbf{w}^T(n)\mathbf{x}(n) \tag{1}$$

The residual error $e(n)$ is given by

$$e(n) = d(n) - y'(n) + v(n) \tag{2}$$

where $y'(n) = y(n) * s(n)$ represents secondary cancelling signal, $s(n)$ is the impulse response of $S(z)$, $*$ denotes the discrete convolution operator, and $v(n)$ is the background noise.

The weight vector update equation of the FxNLMS algorithm is given by

$$\mathbf{w}(n+1) = \mathbf{w}(n) + \mu e(n)\frac{\mathbf{x}_f(n)}{\left\|\mathbf{x}_f(n)\right\|^2 + \varepsilon} \tag{3}$$

where $\mathbf{w}(n) = [w_0(n), w_1(n), \ldots, w_{L-1}(n)]^T$ is the weight vector of the adaptive filter. μ is the step-size, and ε is the regularization factor.

Based on the mean square performance analysis in [18] and [24], it is shown that the NLMS algorithm has good transient response, while the steady-state MSD of the LMS algorithm does not depend on the periodic input power. In addition, for cyclostationary input signals, under small step-size conditions, the LMS algorithm can offer smaller steady-state average MSD than the NLMS algorithm at the same convergence rate. We are therefore excited to research a fresh strategy that can combine the distinct advantages of the two algorithms.

III. PROPOSED ALGORITHM

Fig. 2 illustrates the block diagram of the combined-FxNLMS-FxLMS algorithm. Table 1 lists an overview of the proposed algorithm.

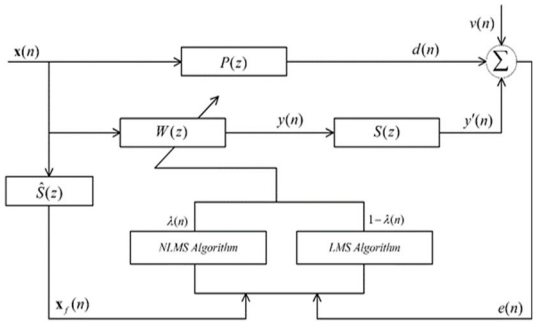

FIGURE 2. Block diagram of the combined-FxNLMS-FxLMS algorithm.

The weight vectors of the FxNLMS algorithm and FxLMS algorithm are updated as follows, where ($\mu_2 < \mu_1$)

$$\mathbf{w}_1(n+1) = \mathbf{w}(n) + \mu_1 e(n) \frac{\mathbf{x}_f(n)}{\left\|\mathbf{x}_f(n)\right\|^2 + \varepsilon} \tag{4}$$

$$\mathbf{w}_2(n+1) = \mathbf{w}(n) + \mu_2 e(n) \mathbf{x}_f(n) \tag{5}$$

combination (4) and (5) yields

$$\mathbf{w}(n+1) = \lambda(n)\mathbf{w}_1(n+1) + (1-\lambda(n))\mathbf{w}_2(n+1) \tag{6}$$

$$\mathbf{w}(n+1) = \mathbf{w}(n) + \left(\frac{\lambda(n)\mu_1}{\left\|\mathbf{x}_f(n)\right\|^2 + \varepsilon} + (1-\lambda(n))\mu_2 \right) e(n)\mathbf{x}_f(n) \tag{7}$$

where $\lambda(n)$ is the mixing parameter in the range [0,1]. It is not difficult to see that when $\lambda(n) \to 1$, the algorithm becomes the FxNLMS algorithm, when $\lambda(n) \to 0$, the algorithm becomes the FxLMS algorithm.

The weight error vector $\tilde{\mathbf{w}}(n)$ is defined as

$$\tilde{\mathbf{w}}(n) = \mathbf{w}_{opt} - \mathbf{w}(n) \tag{8}$$

where $\mathbf{w}_{opt}$ is the optimal weight vector.

Subtracting (7) from $\mathbf{w}_{opt}$ gives rise to

$$\tilde{\mathbf{w}}(n+1) = \tilde{\mathbf{w}}(n) - \left(\frac{\lambda(n)\mu_1}{\left\|\mathbf{x}_f(n)\right\|^2 + \varepsilon} + (1-\lambda(n))\,\mu_2 \right) e(n)\mathbf{x}_f(n) \tag{9}$$

The posteriori error $e_p(n)$ and the priori error $e_a(n)$ are defined as

$$e_p(n) = \mathbf{x}_f^T(n)\tilde{\mathbf{w}}(n+1) \tag{10}$$

$$e_a(n) = \mathbf{x}_f^T(n)\tilde{\mathbf{w}}(n) \tag{11}$$

Assuming perfect modeling of the secondary path, i.e., $\hat{S}(z) = S(z)$, multiplying (9) by $\mathbf{x}_f^T(n)$ yields

$$e_p(n) = e_a(n) - \left(\lambda(n)\mu_1 + (1-\lambda(n))\,\mu_2 \left\|\mathbf{x}_f(n)\right\|^2\right) e(n) \tag{12}$$

Substituting $e(n) = e_a(n) + v(n)$ into (12) yields

$$e_p(n) = e_a(n)\left[1 - \left(\lambda(n)\mu_1 + (1-\lambda(n))\,\mu_2 \left\|\mathbf{x}_f(n)\right\|^2\right)\right] - \left(\lambda(n)\mu_1 + (1-\lambda(n))\,\mu_2 \left\|\mathbf{x}_f(n)\right\|^2\right) v(n) \tag{13}$$

Before going a step further, we need to make some assumptions:

Assumption 1: $\mathbf{x}_f^T(n)$ and the priori error $e_a(n)$ are independent of the background noise $v(n)$ [27].

Assumption 2: The expectation of the ratio of random variables x and y can be approximated by the ratio of their expectation values, i.e., $E[x/y] \approx E[x]/E[y]$ [28].

Taking the square and expectation of (13), and simplifying by above assumptions yields

$$E\left[e_p^2(n)\right] = E\left\{e_a^2(n)\left[1 - \left(\lambda(n)\mu_1 + (1-\lambda(n))\,\mu_2 \left\|\mathbf{x}_f(n)\right\|^2\right)\right]^2\right\} + E\left\{\left(\lambda(n)\mu_1 + (1-\lambda(n))\,\mu_2 \left\|\mathbf{x}_f(n)\right\|^2\right)^2 v^2(n)\right\} \tag{14}$$

Taking the first-order derivative of $\lambda(n)$ for (14) and making its derivative zero yields (15), as shown at the bottom of the next page, where $E[||\mathbf{x}_f(n)||^2] = \sigma^2_{\mathbf{x}_f}(n)$ and $E[e_a^2(n)] = \sigma^2_{e_a}(n)$.

We estimate the variance of the filtered input signal $\sigma^2_{\mathbf{x}_f}(n)$ by the time-average of the squares of $\mathbf{x}_f(n)$

$$\sigma^2_{\mathbf{x}_f}(n) = \alpha_1 \sigma^2_{\mathbf{x}_f}(n-1) + (1-\alpha_1)\left\|\mathbf{x}_f(n)\right\|^2 \tag{16}$$

Next, we approximate the power of noise-free a priori error $\sigma^2_{e_a}(n)$ in (15) by the time-average of the squares of $e_a(n)$

$$\sigma^2_{e_a}(n) = \alpha_1 \sigma^2_{e_a}(n-1) + (1-\alpha_1) e_a^2(n) \tag{17}$$

where α_1 denotes the forgetting factor taking the approximate value of one, and by using the shrinkage denoising method described in [19], the $e_a(n)$ can be obtained

$$e_a(n) = sign(e(n))\max(|e(n)| - t, 0) \tag{18}$$

where $sign(\cdot)$ denotes the signum function, and $t = \sqrt{\theta\sigma_v^2}$, where θ is a constant ($0 \leq \theta \leq 4$) [19].

If the variance of the background noise is unknown in advance, we can find its estimate using the following strategy [29]

$$\sigma_v^2 = \sigma_e^2(n) - E\left[\tilde{\mathbf{w}}^T(n)\,\mathbf{x}_f(n)\,\mathbf{x}_f^T(n)\,\tilde{\mathbf{w}}(n)\right]$$

TABLE 1. Summary of the proposed combined-FxNLMS-FxLMS algorithm.

Initialization	Adaptive process
$\mathbf{w}(0), \theta$	*for* n=0, 1, 2, …
α_1	$\sigma^2_{\mathbf{x}_f}(n) = \alpha_1 \sigma^2_{\mathbf{x}_f}(n-1) + (1-\alpha_1)\left\|\mathbf{x}_f(n)\right\|^2$
α_1	$\sigma^2_{e_a}(n) = \alpha_1 \sigma^2_{e_a}(n-1) + (1-\alpha_1) e_a^2(n)$
$\alpha_1, \sigma_v^2, \lambda_{\min}$	$\lambda(n) = \begin{cases} \alpha_1\lambda(n-1) + (1-\alpha_1)\min\left\{\dfrac{\mu_2\sigma^2_{\mathbf{x}_f}\sigma_v^2 - \sigma^2_{e_a} + \mu_2\sigma^2_{\mathbf{x}_f}\sigma^2_{e_a}}{\mu_2\sigma^2_{\mathbf{x}_f}\sigma^2_{e_a} + \mu_2\sigma^2_{\mathbf{x}_f}\sigma_v^2 - \mu_1(\sigma^2_{e_a}+\sigma_v^2)}, \lambda(n-1)\right\} & \text{if } \lambda(n) > 0 \\ \lambda_{\min} & \text{otherwise} \end{cases}$
$\mu_1,\ \mu_2\ (\mu_2 < \mu_1)$	$\mathbf{w}(n+1) = \mathbf{w}(n) + \left(\dfrac{\lambda(n)\mu_1}{\left\|\mathbf{x}_f(n)\right\|^2 + \varepsilon} + \left(1-\lambda(n)\right)\mu_2\right) e(n)\mathbf{x}_f(n)$

$$\approx \sigma_e^2(n) - \frac{\mathbf{r}^T_{\mathbf{x}_f e}(n)\,\mathbf{r}_{\mathbf{x}_f e}(n)}{\sigma^2_{x_f}(n)} \tag{19}$$

$$\sigma_e^2(n) = \alpha_1\sigma_e^2(n-1) + (1-\alpha_1)\,e^2(n) \tag{20}$$

$$\mathbf{r}_{\mathbf{x}_f e}(n) = \alpha_1 \mathbf{r}_{\mathbf{x}_f e}(n-1) + (1-\alpha_1)\,\mathbf{x}_f(n)\,e(n) \tag{21}$$

We use the time-average method to update $\lambda(n)$. This method not only updates $\lambda(n)$ smoothly but also ensures that it is monotonically decreasing. To avoid $\lambda(n)$ dropping to a negative value, we add a determination condition to overcome this drawback, and the rule for updating is as follows (22), shown at the bottom of the next page.

IV. PERFORMANCE ANALYSIS

A. MEAN SQUARE CONVERGENCE ANALYSIS

The weight error correlation matrix of the combined-FxNLMS-FxLMS algorithm is defined as

$$\mathbf{K}(n) = E\{\tilde{\mathbf{w}}(n)\tilde{\mathbf{w}}^T(n)\} \tag{23}$$

Multiplying (9) by $\tilde{w}^{\mathbf{T}}(n+1)$, taking the expectation, and simplifying by **Assumption** 1, 2 yields (24), as shown at the bottom of the next page, where $\mathbf{R}_f(n) = E\{\mathbf{x}_f(n)\mathbf{x}_f^T(n)\}$ is defined as the correlation matrix of the $\mathbf{x}_f(n)$.

According to $MSD(n) = Tr(\mathbf{K}(n))$, taking the trace of (24) yields (25), as shown at the bottom of the next page.

The trace operation of the matrix is approximated as follows [30]

$$Tr(\mathbf{K}(n)\mathbf{R}_f(n)) \approx \frac{1}{L} Tr(\mathbf{R}_f(n)) Tr(\mathbf{K}(n))$$

$$\approx \frac{1}{L}\sigma^2_{x_f} Tr(\mathbf{K}(n)) \tag{26}$$

$$Tr(\mathbf{R}_f(n)\mathbf{K}(n)\mathbf{R}_f(n)) \approx (\frac{1}{L}Tr(\mathbf{R}_f(n)))^2 Tr(\mathbf{K}(n))$$
$$\approx (\frac{1}{L}\sigma^2_{x_f})^2 Tr(\mathbf{K}(n)) \tag{27}$$

Using the above approximation, (25) can be reduced to

$$\begin{aligned} &MSD(n+1) \\ &= MSD(n) - 2\left(\frac{E\{\lambda(n)\}\,\mu_1}{\sigma^2_{x_f}(n)} + E\{1-\lambda(n)\}\,\mu_2\right) \\ &\quad \times \frac{1}{L}\sigma^2_{x_f}(n) MSD(n) + E\left\{\lambda^2(n)\right\}\mu_1^2\frac{1}{L}MSD(n) \\ &\quad + E\left\{(1-\lambda(n))^2\right\}\mu_2^2\left(\frac{1}{L}\sigma^2_{x_f}(n)\right)^2 (L+2)MSD(n) \\ &\quad + 2E\{\lambda(n)(1-\lambda(n))\}\,\mu_1\mu_2\frac{1}{L}\sigma^2_{x_f}(n)\left(1+\frac{2}{L}\right)MSD(n) \\ &\quad + E\left\{\lambda^2(n)\right\}\mu_1^2\frac{L}{(L+2)\sigma^2_{x_f}(n)}\sigma_v^2(n) + E\left\{(1-\lambda(n))^2\right\} \\ &\quad \times \mu_2^2\sigma^2_{x_f}(n)\sigma_v^2(n) \\ &\quad + 2E\{\lambda(n)(1-\lambda(n))\}\,\mu_1\mu_2\sigma_v^2(n) \end{aligned} \tag{28}$$

when the algorithm reaches the steady state, $\lambda(n)$ tends to zero, so the steady-state MSD value of the algorithm is obtained

$$MSD(\infty) = \frac{\mu_2 L\sigma_v^2}{2 - \mu_2\sigma^2_{x_f}(L+2)} \tag{29}$$

$$\begin{aligned} \lambda(n) &= \frac{E\left\{\mu_2\left\|\mathbf{x}_f(n)\right\|^2 v^2(n) - e_a^2(n) + \mu_2\left\|\mathbf{x}_f(n)\right\|^2 e_a^2(n)\right\}}{E\left\{\mu_2\left\|\mathbf{x}_f(n)\right\|^2 e_a^2(n) + \mu_2\left\|\mathbf{x}_f(n)\right\|^2 v^2(n) - \mu_1\left(e_a^2(n) + v^2(n)\right)\right\}} \\ &= \frac{\mu_2\sigma^2_{\mathbf{x}_f}\sigma_v^2 - \sigma^2_{e_a} + \mu_2\sigma^2_{\mathbf{x}_f}\sigma^2_{e_a}}{\mu_2\sigma^2_{\mathbf{x}_f}\sigma^2_{e_a} + \mu_2\sigma^2_{\mathbf{x}_f}\sigma_v^2 - \mu_1(\sigma^2_{e_a}+\sigma_v^2)} \end{aligned} \tag{15}$$

The analysis of the above equations shows that the algorithm proposed in this paper has the steady-state advantage of the FxLMS algorithm, during the steady-state subject to the step-size μ_2.

B. COMPUTATIONAL COMPLEXITY ANALYSIS

Table 2 provides a comparison of the number of multiplication, addition, and comparison operations required for each iteration of the FxLMS, FxNLMS, VSS FxLMS [9], CFxLMS [10], CVX-FxNLMS-FxLMS [17], CSS FxNLMS [18] algorithms, and the proposed algorithm, where L is the adaptive filter length and M is the secondary channel length.

In each iteration, the proposed algorithm exhibits significantly lower computational complexity compared to the CVX-FxNLMS-FxLMS algorithm. Although the computa-tional complexity of the proposed algorithm increases somewhat when compared to other algorithms, the increase is acceptable and can be compensated by a substantial improvement in convergence speed and noise reduction performance. As such, the proposed algorithm can be considered a promising approach.

V. SIMULATIONS

The performance of the proposed algorithm in the ANC system was evaluated through simulation experiments. FIR filters with the length of $N = 42$ and $M = 10$ are selected to model the primary and secondary paths. Their frequency responses are shown in Fig. 3. Table 3 presents the parameter

$$\lambda(n) = \begin{cases} if\ \lambda(n) > 0 \\ \alpha_1\lambda(n-1) + (1-\alpha_1)\min\left\{ \dfrac{\mu_2\sigma^2_{\mathbf{x}_f}(n)\sigma^2_v(n) - \sigma^2_{e_a}(n) + \mu_2\sigma^2_{\mathbf{x}_f}(n)\sigma^2_{e_a}(n)}{\mu_2\sigma^2_{\mathbf{x}_f}(n)\sigma^2_{e_a}(n) + \mu_2\sigma^2_{\mathbf{x}_f}(n)\sigma^2_v(n) - \mu_1\left(\sigma^2_{e_a}(n) + \sigma^2_v(n)\right)}, \lambda(n-1) \right\} \\ \lambda_{\min} \end{cases} \tag{22}$$

$$\begin{aligned} \mathbf{K}(n+1) = {} & \mathbf{K}(n) - E\{\lambda(n)\}\mu_1\mathbf{K}(n)\frac{\mathbf{R}_f(n)}{Tr(\mathbf{R}_f(n))} - E\{\lambda(n)\}\mu_1\frac{\mathbf{R}_f(n)}{Tr(\mathbf{R}_f(n))}\mathbf{K}(n) \\ & - E\{1-\lambda(n)\}\mu_2\mathbf{K}(n)\mathbf{R}_f(n) - E\{1-\lambda(n)\}\mu_2\mathbf{R}_f(n)\mathbf{K}(n) \\ & + E\{\lambda^2(n)\}\mu_1^2\frac{Tr(\mathbf{K}(n)\mathbf{R}_f(n))\mathbf{R}_f(n) + 2\mathbf{R}_f(n)\mathbf{K}(n)\mathbf{R}_f(n)}{\{Tr(\mathbf{R}_f(n))\}^2 + 2Tr(\mathbf{R}_f(n)\mathbf{R}_f(n))} \\ & + E\{(1-\lambda(n))^2\}\mu_2^2(Tr(\mathbf{K}(n)\mathbf{R}_f(n))\mathbf{R}_f(n) + 2\mathbf{R}_f(n)\mathbf{K}(n)\mathbf{R}_f(n)) \\ & + 2E\{\lambda(n)(1-\lambda(n))\}\mu_1\mu_2\frac{Tr(\mathbf{K}(n)\mathbf{R}_f(n))\mathbf{R}_f(n) + 2\mathbf{R}_f(n)\mathbf{K}(n)\mathbf{R}_f(n)}{Tr(\mathbf{R}_f(n))} \\ & + E\{\lambda^2(n)\}\mu_1^2\frac{\mathbf{R}_f(n)}{\{Tr(\mathbf{R}_f(n))\}^2 + 2Tr(\mathbf{R}_f(n)\mathbf{R}_f(n))}\sigma_v^2 \\ & + E\{(1-\lambda(n))^2\}\mu_2^2\mathbf{R}_f(n)\sigma_v^2 \\ & + 2E\{\lambda(n)(1-\lambda(n))\}\mu_1\mu_2\frac{\mathbf{R}_f(n)}{Tr(\mathbf{R}_f(n))}\sigma_v^2 \end{aligned} \tag{24}$$

$$\begin{aligned} MSD(n+1) = {} & Tr(\mathbf{K}(n+1)) \\ = {} & Tr(\mathbf{K}(n)) - 2E\{\lambda(n)\}\mu_1\frac{Tr(\mathbf{R}_f(n)\mathbf{K}(n))}{Tr(\mathbf{R}_f(n))} \\ & - E\{1-\lambda(n)\}\mu_2 Tr(\mathbf{K}(n)\mathbf{R}_f(n)) - E\{1-\lambda(n)\}\mu_2 Tr(\mathbf{R}_f(n)\mathbf{K}(n)) \\ & + E\{\lambda^2(n)\}\mu_1^2\frac{Tr(\mathbf{K}(n)\mathbf{R}_f(n))Tr(\mathbf{R}_f(n)) + 2Tr(\mathbf{R}_f(n)\mathbf{K}(n)\mathbf{R}_f(n))}{\{Tr(\mathbf{R}_f(n))\}^2 + 2Tr(\mathbf{R}_f(n)\mathbf{R}_f(n))} \\ & + E\{(1-\lambda(n))^2\}\mu_2^2(Tr(\mathbf{K}(n)\mathbf{R}_f(n))Tr(\mathbf{R}_f(n)) + 2Tr(\mathbf{R}_f(n)\mathbf{K}(n)\mathbf{R}_f(n))) \\ & + 2E\{\lambda(n)(1-\lambda(n))\}\mu_1\mu_2\frac{Tr(\mathbf{K}(n)\mathbf{R}_f(n))Tr(\mathbf{R}_f(n)) + 2Tr(\mathbf{R}_f(n)\mathbf{K}(n)\mathbf{R}_f(n))}{Tr(\mathbf{R}_f(n))} \\ & + E\{\lambda^2(n)\}\mu_1^2\frac{Tr(\mathbf{R}_f(n))}{\{Tr(\mathbf{R}_f(n))\}^2 + 2Tr(\mathbf{R}_f(n)\mathbf{R}_f(n))}\sigma_v^2 \\ & + E\{(1-\lambda(n))^2\}\mu_2^2 Tr(\mathbf{R}_f(n))\sigma_v^2 + 2E\{\lambda(n)(1-\lambda(n))\}\mu_1\mu_2\sigma_v^2 \end{aligned} \tag{25}$$

TABLE 2. Computational complexity.

Algorithms	Multiplications	Additions	Comparisons
FxLMS	$2L+2M+1$	$2L+2M-2$	0
FxNLMS	$3L+2M+2$	$3L+2M-2$	0
VSS FxLMS	$3L+2M+7$	$3L+2M+3$	0
CFxLMS	$3L+2M+6$	$3L+2M+3$	0
CVX-FxNLMS-FxLMS	$5L+4M+17$	$5L+4M+5$	2
CSS-FxNLMS	$3L+2M+9$	$3L+2M+4$	1
Proposed	$3L+2M+11$	$3L+2M+6$	2

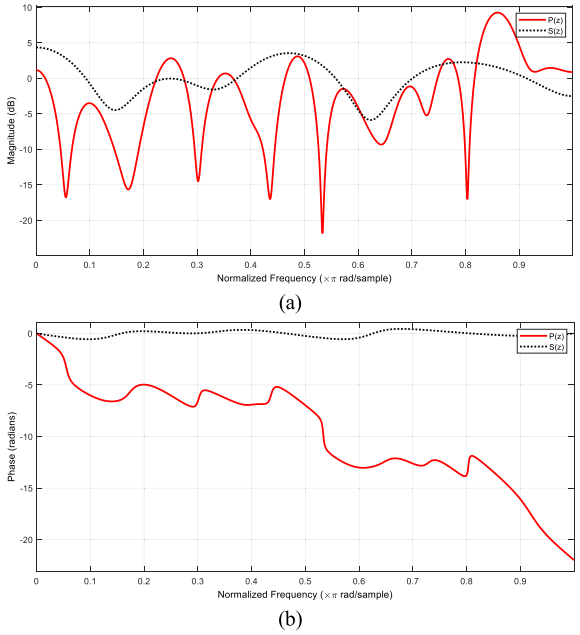

FIGURE 3. Frequency response of acoustic paths used in computer simulations. (a) Magnitude response; (b) Phase response.

settings for each algorithm used in all simulation experiments in this article (The symbol "/" indicates that the algorithm has not been configured.).

The Average Noise Reduction (ANR), Mean Squared Deviation (MSD), and Sound Pressure Level (SPL), as an evaluation index to evaluate the performance of active noise control systems.

The Average Noise Reduction (ANR) is defined as

$$ANR(n)(dB) = 20\log_{10}\left(\frac{A_e(n)}{A_d(n)}\right) \tag{30}$$

where $A_e(n) = \kappa A_e(n\text{-}1)+(1)\text{-}\kappa)|e(n)|$, $A_d(n) = \kappa A_d(n\text{-}1)+(1)\text{-}\kappa)|d(n)|$. In the initial condition, $A_e(n) = 0$, $A_d(n) = 0$, $\kappa = 0.999$.

The Sound Pressure Level (SPL) is defined as [31]

$$SPL(dB) = 20\log_{10}\left(\frac{P}{P_{ref}}\right) \tag{31}$$

where, P is sound pressure, P_{ref} is the reference sound pressure and $P_{ref} = 2 \times 10^{-5}$ Pa.

A. SIMULATING CYCLOSTATIONARY NOISE

In this section, we utilize the sinusoidal power time variation from [18] and [30] to create simulated cyclostationary noise signals, i.e.,

$$\sigma_x^2(n) = \beta\left(1+\sin\left(\frac{\omega_0\pi n}{2}\right)\right) \tag{32}$$

where $\beta > 0$, $\omega_0 > 0$. In the subsequent simulation experiments, the parameter settings are as follows: $\beta = 0.0196$, $\omega_0 = 0.0625$. Fig. 4 illustrates the waveform and three-dimensional cyclic spectrum of the noise signal.

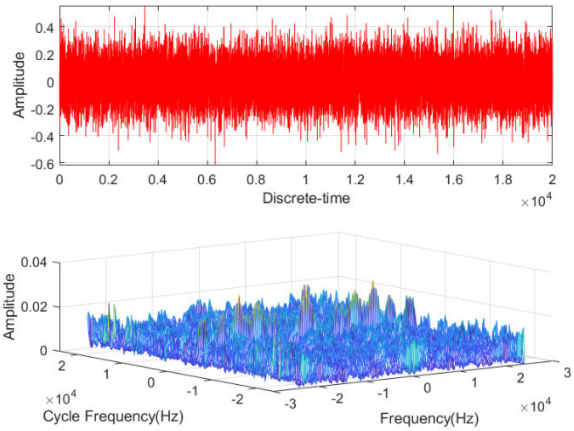

FIGURE 4. Waveform diagram and Three-dimensional cyclic spectrum of the noise signal.

To verify the effectiveness and reliability of the proposed algorithm, its performance was compared with FxNLMS, FxLMS, VSS FxLMS, CFxLMS, CVX-FxNLMS FxLMS, and CSS FxNLMS algorithms. The MSD learning curves and ANR learning curves of the aforementioned algorithms are shown in Fig. 5 and Fig. 6, respectively.

After comparing the MSD convergence curves of each algorithm in Fig. 5, it was found that the proposed algorithm achieved a good balance between convergence speed and noise reduction accuracy. When compared with the FxNLMS algorithm, they exhibited similar convergence speeds; compared with the FxLMS algorithm, they maintained similar denoising accuracy. While the proposed algorithm exhibited similar noise reduction accuracy to the CVX-FxNLMS-FxLMS algorithm and CSS-FxNLMS algorithm, it significantly outperformed other algorithms in terms of convergence

TABLE 3. Tuning parameters of the algorithms.

FIGURE	FxLMS	FxNLMS	VSS FxLMS	CFxLMS	CVX-FxNLMS-FxLMS	CSS-FxNLMS	Proposed
FIGURE 5	μ=1	μ=0.05	a=0.5, b=0.1, c=1	α=5, β=0.05, γ= 0.1	μ_1=1, μ_2=0.005, η=0.99, a^+=4	μ_1=1, μ_2=0.05, Q=1, α_1=0.996	μ_1=1, μ_2=0.05, θ=1, α_1=0.996, λ_{min}=10^{-6}
FIGURE 6	μ=1	μ=0.05	a=0.5, b=0.1, c=1	α=5, β=0.05, γ= 0.1	μ_1=1, μ_2=0.005, η=0.99, a^+=4	μ_1=1, μ_2=0.05, Q=1, α_1=0.996	μ_1=1, μ_2=0.05, θ=1, α_1=0.996, λ_{min}=10^{-6}
FIGURE 8	μ=1.5	μ=0.05	/	/	/	/	μ_1=1.5, μ_2=0.05, θ=1, α_1=0.996, λ_{min}=10^{-6}
FIGURE 9	μ=1.5	μ=0.05	/	/	/	/	μ_1=1.5, μ_2=0.05, θ=1, α_1=0.996, λ_{min}=10^{-6}
FIGURE 10	μ=1.5	μ=0.05	a=5, b=0.03, c=2	α=15, β=0.01, γ= 0.7	μ_1=1.5, μ_2=0.05, η=0.99, a^+=4	μ_1=1.5, μ_2=0.05, Q=1, α_1=0.996	μ_1=1.5, μ_2=0.05, θ=1, α_1=0.996, λ_{min}=10^{-6}
FIGURE 11	μ=1.5	μ=0.05	a=5, b=0.03, c=2	α=15, β=0.01, γ= 0.7	μ_1=1.5, μ_2=0.05, η=0.99, a^+=4	μ_1=1.5, μ_2=0.05, Q=1, α_1=0.996	μ_1=1, μ_2=0.05, θ=1, α_1=0.996, λ_{min}=10^{-6}
FIGURE 12	μ=1.5	μ=0.05	a=5, b=0.03, c=2	α=15, β=0.01, γ= 0.7	μ_1=1.5, μ_2=0.05, η=0.99, a^+=4	μ_1=1.5, μ_2=0.05, Q=1, α_1=0.996	μ_1=1.5, μ_2=0.05, θ=1, α_1=0.996, λ_{min}=10^{-6}
FIGURE 13	μ=1.5	μ=0.05	a=5, b=0.05, c=1	α=15, β=0.09, γ= 0.8	μ_1=1.5, μ_2=0.05, η=0.99, a^+=4	μ_1=1.5, μ_2=0.05, Q=1, α_1=0.996	μ_1=1.5, μ_2=0.05, θ=1, α_1=0.996, λ_{min}=10^{-6}
FIGURE 14	μ=1.5	μ=0.05	a=5, b=0.05, c=1	α=15, β=0.09, γ= 0.8	μ_1=1.5, μ_2=0.05, η=0.99, a^+=4	μ_1=1.5, μ_2=0.05, Q=1, α_1=0.996	μ_1=1.5, μ_2=0.05, θ=1, α_1=0.996, λ_{min}=10^{-6}
FIGURE 15	/	/	/	/	/	/	μ_1=1.5, μ_2=0.05, θ=1, α_1=0.997, λ_{min}=10^{-6}

speed. Moreover, the ANR convergence curves of each algorithm in Fig. 6 also demonstrated similar results, which further verified the reliability and effectiveness of the proposed algorithm. Overall, these analysis results suggest that the proposed algorithm has superior overall performance.

B. REAL SAMPLING CYCLOSTATIONARY NOISE

To further validate the effectiveness and reliability of the proposed algorithm, this section utilizes automotive engine noise signals obtained through real sampling. The sampling frequency used is 48kHz. Fig. 7 illustrates the waveform and three-dimensional cyclic spectrum of the noise signal. The noise signal satisfies the condition of non-zero cyclic autocorrelation function when the cyclic frequency is not zero, indicating its cyclostationary properties. The background noise, on the other hand, is represented by Gaussian white noise that is independent of the reference signal.

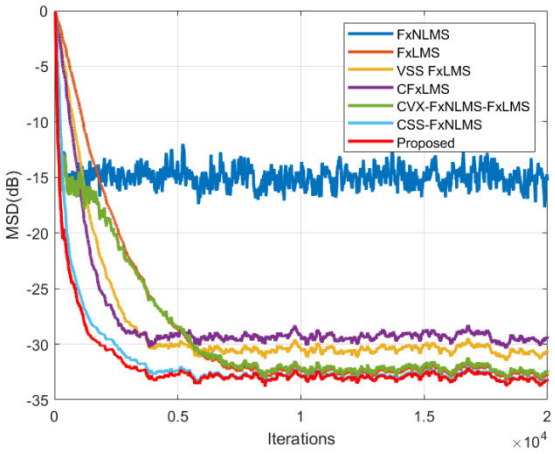

FIGURE 5. MSD learning curves of the FxNLMS, FxLMS, VSS FxLMS, CFxLMS, CVX-FxNLMS-FxLMS, CSS FxNLMS and the Proposed algorithm in an environment with SNR = 15dB.

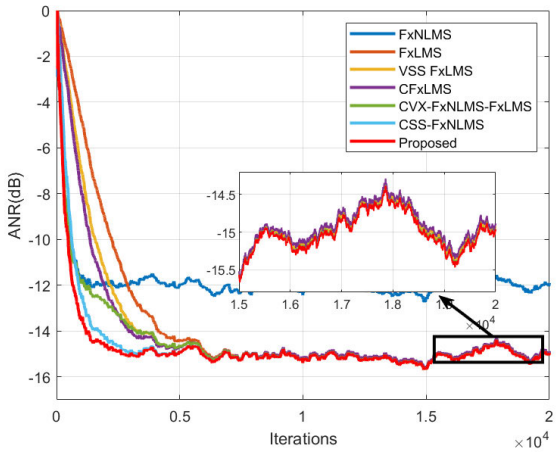

FIGURE 6. ANR learning curves of the FxNLMS, FxLMS, VSS FxLMS, CFxLMS, CVX-FxNLMS-FxLMS, CSS FxNLMS and the Proposed algorithm in an environment with SNR=15dB.

To verify the tracking ability of the proposed algorithm, we conducted experiments to determine whether it can adaptively adjust with changes in the external environment. Specifically, we simulated a non-stationary environment by multiplying the impulse response of the main path $P(z)$ by -1 when the algorithm reached 8000 iterations [32]. Fig. 8 illustrates the learning curve of the mixing parameter $\lambda(n)$ in a non-stationary environment, while Fig. 9 displays the ANR performance curve of the proposed algorithm in the same environment. These figures demonstrate that the mixing parameter $\lambda(n)$ can dynamically update its value in response to changes in the external environment, ensuring it remains within the range of 0 to 1. This adaptability guarantees the excellent performance of the proposed algorithm in non-stationary environments.

The comparison results of the MSD learning curves and ANR learning curves between the proposed algorithm and other similar algorithms are displayed in Fig. 10 and Fig. 11, respectively.

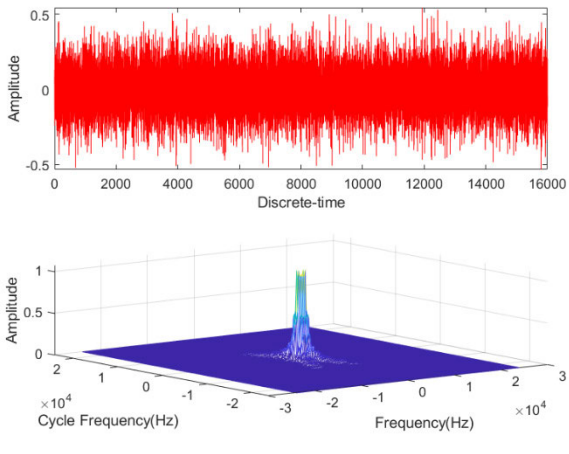

FIGURE 7. Waveform diagram and Three-dimensional cyclic spectrum of the noise signal.

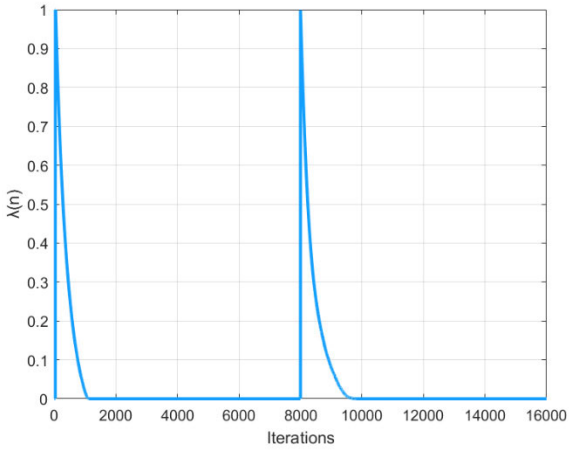

FIGURE 8. Variation curve of the mixing parameter in a non-stationary environment.

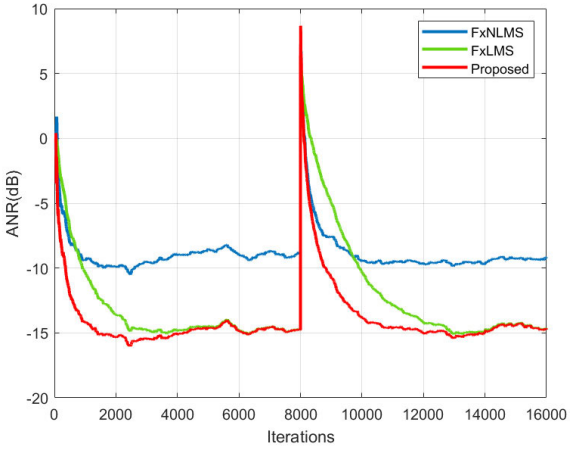

FIGURE 9. ANR learning curve of the Proposed algorithm in a non-stationary environment.

By comparing and analyzing the MSD learning curves of each algorithm in Fig. 10, it is evident that all algorithms exhibit stable convergence and effectively reduce noise

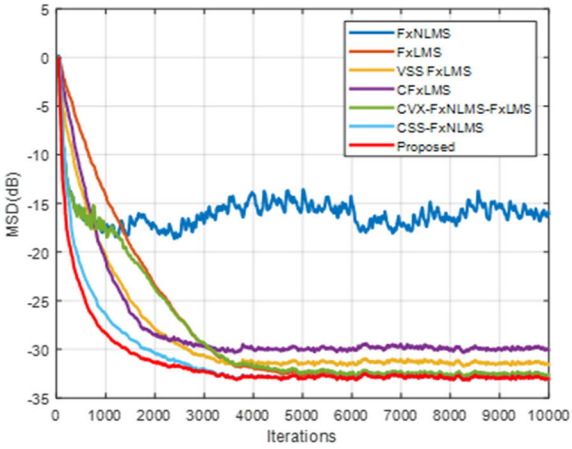

FIGURE 10. MSD learning curves of the FxNLMS, FxLMS, VSS FxLMS, CFxLMS, CVX-FxNLMS-FxLMS, CSS FxNLMS and the Proposed algorithm in an environment with SNR=20dB.

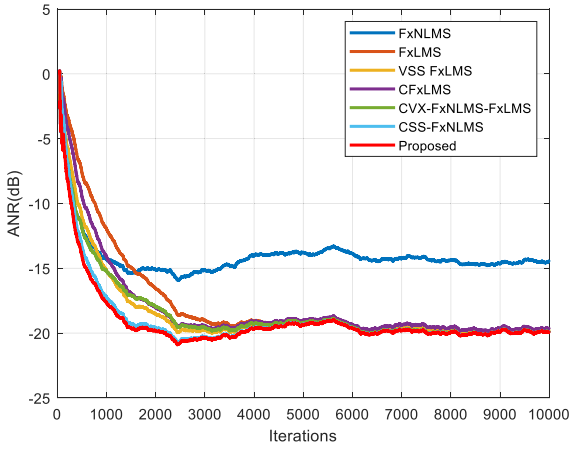

FIGURE 11. ANR learning curves of the FxNLMS, FxLMS, VSS FxLMS, CFxLMS, CVX-FxNLMS-FxLMS, CSS FxNLMS and the Proposed algorithm in an environment with SNR=20dB.

signals. The proposed algorithm, in particular, demonstrates a favorable overall performance by combining the strengths of the FxNLMS algorithm and the FxLMS algorithm. It achieves rapid convergence while maintaining excellent noise reduction accuracy. Although the proposed algorithm performs similarly to the CSS-FxNLMS algorithm in terms of noise reduction accuracy, it holds a slight advantage in terms of convergence speed. The comparison results in Fig. 11 further validate this viewpoint, which is consistent with the comparative analysis results presented in the previous section. This provides additional confirmation of the reliability of the proposed algorithm.

To provide a more intuitive demonstration of the level of noise attenuation achieved by each algorithm, Fig. 12 displays the SPL curves of the noise signal after being processed by an ANC system employing different algorithms. It is evident that the noise signal has been effectively attenuated to a certain degree through the implementation of ANC systems using various algorithms. Notably, the ANC system utilizing the proposed algorithm achieves the maximum reduction in

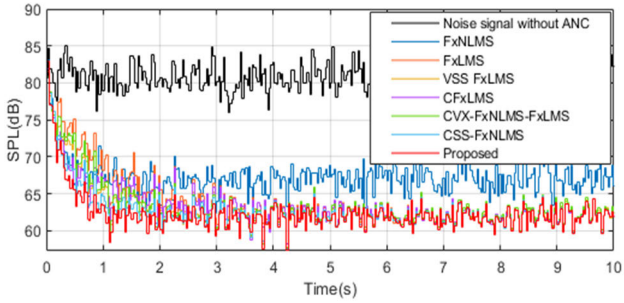

FIGURE 12. SPL curves of the FxNLMS, FxLMS, VSS FxLMS, CFxLMS, CVX-FxNLMS- FxLMS, CSS FxNLMS and the Proposed algorithm in an environment with SNR=20dB.

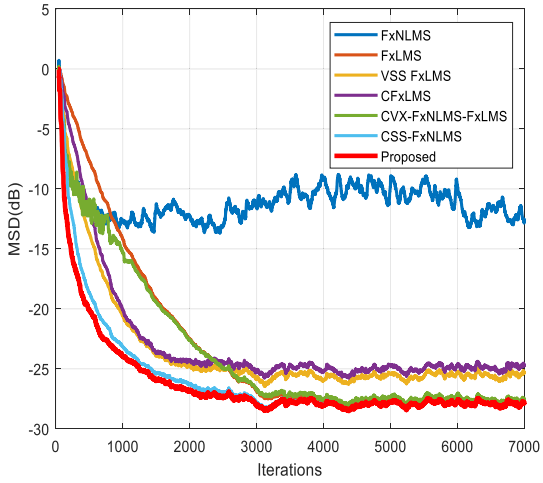

FIGURE 13. MSD learning curves of the FxNLMS, FxLMS, VSS FxLMS, CFxLMS, CVX-FxNLMS-FxLMS, CSS FxNLMS and the Proposed algorithm in an environment with SNR=15dB.

SPL while maintaining a faster denoising speed compared to other algorithms.

Furthermore, to confirm the performance of the proposed algorithm in different background noise environments, we conducted additional experiments. Fig. 13 illustrates the MSD learning curves with all other environmental factors remaining constant, except for an SNR of 15dB. Additionally, Fig. 14 displays the performance curves of the algorithm when the SNR is 30dB. It is evident that the proposed algorithm maintains excellent performance in both the above mentioned SNR environments, which fully verifies our hypothesis that the proposed algorithm is effective in various background noise environments.

Finally, to validate the accuracy of the theoretical analysis on the mean square convergence performance of the proposed algorithm in the fourth section, we conducted experimental verification. As depicted in Fig. 15, the theoretical MSD curve and the simulated MSD curve exhibited good consistency, confirming the consistency of both transient and steady-state behavior. However, it is worth noting that there exists a slight deviation between the theoretical and simulated MSD in terms of transient behavior. Such deviations

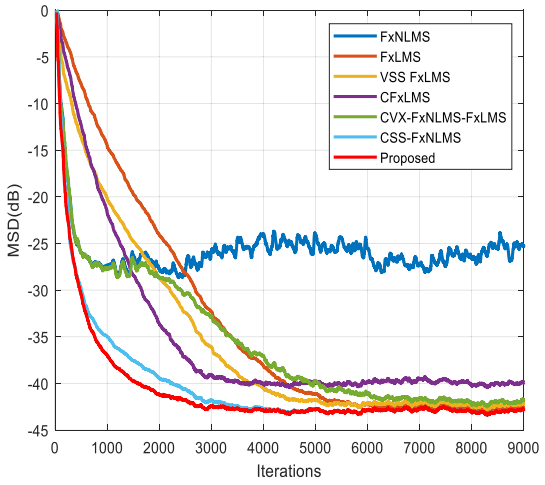

FIGURE 14. MSD learning curves of the FxNLMS, FxLMS, VSS FxLMS, CFxLMS, CVX-FxNLMS-FxLMS, CSS FxNLMS and the Proposed algorithm in an environment with SNR=30dB.

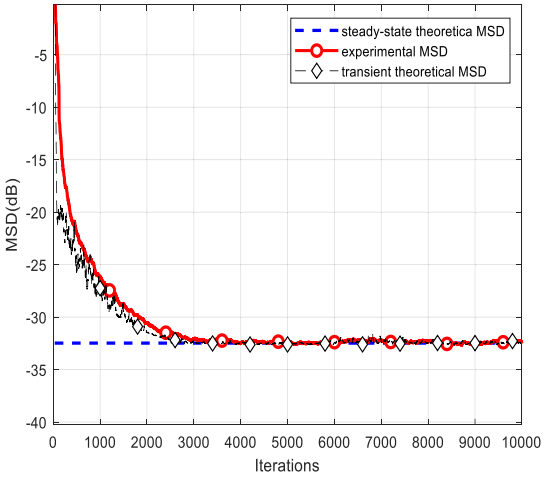

FIGURE 15. Transient theoretical MSD, experimental MSD, and steady-state theoretical MSD of the Proposed algorithm in an environment with SNR=20dB.

are expected since certain approximations from the literature were utilized in the analysis [28], [30].

VI. CONCLUSION

A new combined-FxNLMS-FxLMS algorithm for feedforward ANC systems with the cyclostationary noise inputs is proposed in this paper. In the proposed algorithm, a larger step size is used for FxNLMS to achieve fast convergence, and the smaller one is used in FxLMS for getting low steady-state MSD. The mixing parameter is obtained by minimizing the energy of a posteriori error, which is updated by employing the moving average method to ensure the monotonically decreasing while avoiding large fluctuations. Additionally, the mean square convergence performance and computational complexity of the proposed algorithm are performed, and simulation studies demonstrate the strong concordance between theory and practice. The results of the simulation demonstrate that the combined-FxNLMS-FxLMS algorithm effectively amalgamates the advantages of the FxNLMS algorithm and the FxLMS algorithm showcasing exceptional noise reduction capabilities.

REFERENCES

[1] S. J. Elliott and P. A. Nelson, "Active noise control," *IEEE Signal Process. Mag.*, vol. 10, no. 4, pp. 12–35, Oct. 1993.

[2] G. Lu, R. Chen, and H. Liu, "Active noise control scheme for smart beds based on a wide and narrow band hybrid control algorithm," *IEEE Access*, vol. 11, pp. 92617–92627, 2023, doi: 10.1109/ACCESS.2023.3308694.

[3] S. Kim and M. E. Altinsoy, "A complementary effect in active control of powertrain and road noise in the vehicle interior," *IEEE Access*, vol. 10, pp. 27121–27135, 2022, doi: 10.1109/ACCESS.2022.3157449.

[4] Y. K. Bharath and S. Veena, "Dynamic active noise control of broadband noise in fighter aircraft pilot helmet," *Sound Vibration*, vol. 56, no. 4, pp. 319–331, 2022, doi: 10.32604/sv.2022.015634.

[5] E. Noh, S. Woo, D. J. Lee, M.-H. Song, J.-W. Lee, H. Lee, W.-S. Ohm, H. Jang, K. Lee, Y. Park, and Y. Seo, "Active control of low-frequency noise in bubbly water-filled pipes," *J. Mech. Sci. Technol.*, vol. 33, no. 7, pp. 3127–3135, Jul. 2019, doi: 10.1007/s12206-019-0608-3.

[6] W. Yin, Y. Wei, T. Liu, and Y. Wang, "A novel orthogonalized fractional order filtered-x normalized least mean squares algorithm for feedforward vibration rejection," *Mech. Syst. Signal Process.*, vol. 119, pp. 138–154, Mar. 2019, doi: 10.1016/j.ymssp.2018.09.024.

[7] B. Huang, Y. Xiao, J. Sun, and G. Wei, "A variable step-size FXLMS algorithm for narrowband active noise control," *IEEE Trans. Audio, Speech, Language Process.*, vol. 21, no. 2, pp. 301–312, Feb. 2013, doi: 10.1109/TASL.2012.2223673.

[8] D.-C. Chang and F.-T. Chu, "Feedforward active noise control with a new variable tap-length and step-size filtered-X LMS algorithm," *IEEE/ACM Trans. Audio, Speech, Language Process.*, vol. 22, no. 2, pp. 542–555, Feb. 2014, doi: 10.1109/TASLP.2013.2297016.

[9] X. Zhang, S. Yang, Y. Liu, and W. Zhao, "Improved variable step size least mean square algorithm for pipeline noise," *Sci. Program.*, vol. 2022, pp. 1–16, Feb. 2022, doi: 10.1155/2022/3294674.

[10] Y. Ma, Y. Wu, and X. Yang, "CFxLMS algorithm with variable step size and its application to simulation of elevator cabin noise active control," *Noise Vibrat. Control*, vol. 38, no. 5, pp. 57–61, 2018.

[11] Q. Zhang, D. Lin, Y. Xiao, Y. Zheng, and S. Wang, "Error reused Filtered-X least mean square algorithm for active noise control," *IEEE/ACM Trans. Audio, Speech, Language Process.*, vol. 32, pp. 397–412, 2024, doi: 10.1109/TASLP.2023.3330077.

[12] A. Carini and G. L. Sicuranza, "Optimal regularization parameter of the multichannel filtered-*x* affine projection algorithm," *IEEE Trans. Signal Process.*, vol. 55, no. 10, pp. 4882–4895, Oct. 2007, doi: 10.1109/TSP.2007.896113.

[13] J.-M. Song and P. Park, "An optimal variable step-size affine projection algorithm for the modified filtered-*x* active noise control," *Signal Process.*, vol. 114, pp. 100–111, Sep. 2015, doi: 10.1016/j.sigpro.2015.02.005.

[14] A. Mirza, F. Afzal, A. Zeb, A. Wakeel, W. S. Qureshi, and A. Akgul, "New FxLMAT based algorithms for active control of impulsive noise," *IEEE Access*, vol. 11, pp. 81279–81288, 2023, doi: 10.1109/ACCESS.2023.3293647.

[15] Y.-R. Chien, C.-H. Yu, and H.-W. Tsao, "Affine-projection-like maximum correntropy criteria algorithm for robust active noise control," *IEEE/ACM Trans. Audio, Speech, Language Process.*, vol. 30, pp. 2255–2266, 2022.

[16] Z. C. He, H. H. Ye, and E. Li, "An efficient algorithm for nonlinear active noise control of impulsive noise," *Appl. Acoust.*, vol. 148, pp. 366–374, May 2019, doi: 10.1016/j.apacoust.2019.01.003.

[17] M. Ferrer, A. Gonzalez, M. de Diego, and G. Pinero, "Convex combination filtered-X algorithms for active noise control systems," *IEEE Trans. Audio, Speech, Language Process.*, vol. 21, no. 1, pp. 156–167, Jan. 2013, doi: 10.1109/TASL.2012.2215595.

[18] S. Zhang, W. Xing Zheng, and J. Zhang, "A new combined-step-size normalized least mean square algorithm for cyclostationary inputs," *Signal Process.*, vol. 141, pp. 261–272, Dec. 2017, doi: 10.1016/j.sigpro.2017.06.007.

[19] Z. A. Bhotto and A. Antoniou, "A family of shrinkage adaptive-filtering algorithms," *IEEE Trans. Signal Process.*, vol. 61, no. 7, pp. 1689–1697, Apr. 2013, doi: 10.1109/TSP.2012.2236831.

[20] P. Song and H. Zhao, "Filtered-x generalized mixed norm (FXGMN) algorithm for active noise control," *Mech. Syst. Signal Process.*, vol. 107, pp. 93–104, Jul. 2018, doi: 10.1016/j.ymssp.2018.01.035.
[21] A. C. McCormick and A. K. Nandi, "Cyclostationarity in rotating machine vibrations," *Mech. Syst. Signal Process.*, vol. 12, no. 2, pp. 225–242, Mar. 1998, doi: 10.1006/mssp.1997.0148.
[22] Y. Jiang, S. Chen, F. Gu, H. Meng, and Y. Cao, "A modified feedforward hybrid active noise control system for vehicle," *Appl. Acoust.*, vol. 175, Apr. 2021, Art. no. 107816, doi: 10.1016/j.apacoust.2020.107816.
[23] B. Lam, W.-S. Gan, D. Shi, M. Nishimura, and S. Elliott, "Ten questions concerning active noise control in the built environment," *Building Environ.*, vol. 200, Aug. 2021, Art. no. 107928, doi: 10.1016/j.buildenv.2021.107928.
[24] S. Zhang, J. Zhang, and H. C. So, "Mean square deviation analysis of LMS and NLMS algorithms with white reference inputs," *Signal Process.*, vol. 131, pp. 20–26, Feb. 2017, doi: 10.1016/j.sigpro.2016.07.027.
[25] L. Shi, H. Zhao, W. Wang, and L. Lu, "Combined regularization parameter for normalized LMS algorithm and its performance analysis," *Signal Process.*, vol. 162, pp. 75–82, Sep. 2019, doi: 10.1016/j.sigpro.2019.04.014.
[26] E. Pichardo, Á. Vázquez, E. R. Anides, J. C. Sánchez, H. Perez, J. G. Avalos, and G. Sánchez, "A dual adaptive filter spike-based hardware architecture for implementation of a new active noise control structure," *Electronics*, vol. 10, no. 16, p. 1945, Aug. 2021, doi: 10.3390/electronics10161945.
[27] L. Shi, H. Zhao, and Y. Zakharov, "An improved variable kernel width for maximum correntropy criterion algorithm," *IEEE Trans. Circuits Syst. II, Exp. Briefs*, vol. 67, no. 7, pp. 1339–1343, Jul. 2020, doi: 10.1109/TCSII.2018.2880564.
[28] S.-H. Yim, H.-S. Lee, and W.-J. Song, "A proportionate diffusion LMS algorithm for sparse distributed estimation," *IEEE Trans. Circuits Syst. II, Exp. Briefs*, vol. 62, no. 10, pp. 992–996, Oct. 2015, doi: 10.1109/TCSII.2015.2435631.
[29] M. A. Iqbal and S. L. Grant, "Novel variable step size NLMS algorithms for echo cancellation," in *Proc. IEEE Int. Conf. Acoust., Speech Signal Process.*, Mar. 2008, pp. 241–244, doi: 10.1109/ICASSP.2008.4517591.
[30] N. J. Bershad, E. Eweda, and J. C. M. Bermudez, "Stochastic analysis of the LMS and NLMS algorithms for cyclostationary white Gaussian inputs," *IEEE Trans. Signal Process.*, vol. 62, no. 9, pp. 2238–2249, May 2014, doi: 10.1109/TSP.2014.2307278.
[31] E. A. Ntumy and S. V. Utyuzhnikov, "Active sound control in composite regions," *Appl. Numer. Math.*, vol. 93, pp. 242–253, Jul. 2015, doi: 10.1016/j.apnum.2014.04.006.
[32] P. Song and H. Zhao, "Filtered-x least mean square/fourth (FXLMS/F) algorithm for active noise control," *Mech. Syst. Signal Process.*, vol. 120, pp. 69–82, Apr. 2019, doi: 10.1016/j.ymssp.2018.10.009.

YUNHE PANG received the bachelor's degree from Yantai University, Yantai, China, in 2020, where he is currently pursuing the master's degree. His research interests include adaptive filtering algorithm, active noise control, and machine learning.

SHIFENG OU received the Ph.D. degree from Jilin University, Jilin, China, in 2008. He is currently a Professor and a Master Tutor with the School of Physics and Electronic Information, Yantai University, Yantai, China. His research interests include speech signal processing, adaptive filtering algorithm, and blind signal processing.

ZHUORAN CAI (Member, IEEE) received the Ph.D. degree in information and communication engineering from Harbin Institute of Technology, in 2013. He is currently an Associate Professor with the School of Physics and Electronic Information, Yantai University, Yantai, China. His research interests include deep learning methods, cognitive radio, and compressed sensing.

YING GAO received the Ph.D. degree from Jilin University, Jilin, China, in 2008. She is currently an Associate Professor and a Master Tutor with the School of Physics and Electronic Information, Yantai University, Yantai, China. Her main research interest includes signal and information processing.